Nuclear Instruments and Methods in Physics Research A 857 (2017) 66–74

Contents lists available at ScienceDirect

Nuclear Instruments and Methods in Physics Research A

journal homepage: www.elsevier.com/locate/nima

Shape of intrinsic alpha pulse height spectra in lanthanide halide scintillators

W. Wolszczak*, P. Dorenbos

Delft University of Technology, Faculty of Applied Sciences, Department of Radiation Science and Technology (FAME-LMR), Mekelweg 15, 2629 JB Delft, Netherlands

ARTICLE INFO

Keywords:
Scintillator
α/β ratio
Internal activity
^{227}Ac contamination
$LaBr_3$:Ce
$LaBr_3$:Ce,Sr
$CeBr_3$

ABSTRACT

Internal contamination with actinium-227 and its daughters is a serious drawback in low-background applications of lanthanide-based scintillators. In this work we showed the important role of nuclear γ de-excitations on the shape of the internal alpha spectrum measured in scintillators. We calculated with Bateman equations the activities of contamination isotopes and the time evolution of actinium-227 and its progenies. Next, we measured the intrinsic background spectra of $LaBr_3$(Ce), $LaBr_3$(Ce,Sr) and $CeBr_3$ with a digital spectroscopy technique, and we analyzed them with a pulse shape discrimination method (PSD) and a time-amplitude analysis. Finally, we simulated the α background spectrum with Geant4 tool-kit, consequently taking into account complex α-γ-electron events, the α/β ratio dependence on the α energy, and the electron/γ nonproportionality.

We found that α-γ mixed events have higher light yield than expected for alpha particles alone, which leads to overestimation of the α/β ratio when it is measured with internal ^{227}Th and ^{223}Ra isotopes. The time-amplitude analysis showed that the α peaks of ^{219}Rn and ^{215}Po in $LaBr_3$(Ce) and $LaBr_3$(Ce,Sr) are not symmetric. We compared the simulation results with the measured data and provided further evidence of the important role of mixed α-γ-electron events for understanding the shape of the internal α spectrum in scintillators.

1. Introduction

Internal radioactive contamination is a serious drawback of lanthanide-based scintillators in low background applications. It reduces detector sensitivity [1], interferes with neutron measurements [2,3] and complicates data analysis. A high internal background limits the usability of modern lanthanide-based scintillators when high radio-purity is important, for example in dark matter searches [4], gamma measurements in space exploration missions [5], detection of rare events [6,7], and construction of high-sensitivity gamma detectors.

Intrinsic contamination with α and β-decaying isotopes has been found in many lanthanide-based scintillators, for example $LaBr_3$:Ce, $LaCl_3$:Ce [8–10], $CeBr_3$ [1], and $Cs_2LiLaBr_6$:Ce (CLLB) [3]. The sources of the contamination are naturally occurring radioactive isotopes: ^{138}La, ^{227}Ac, and their daughters undergoing α and β^- decays. Natural lanthanum is composed of stable ^{139}La (99.91% abundance) and radioactive ^{138}La [11]. Since it is not possible to separate both isotopes by chemical methods, ^{138}La contamination is unavoidable in scintillators containing lanthanum. Moreover, natural actinium contains a radioactive ^{227}Ac isotope. Actinium and lanthanum have very similar chemical properties, so all lanthanide-based scintillators are subjected to ^{227}Ac isotope contamination. Using cerium instead of lanthanum in cerium bromide makes it possible to obtain much higher radio-purity of the final material [1], but $CeBr_3$ has a lower energy resolution compared to other lanthanide scintillators.

Much research has addressed these issues trying to understand the origin of an internal background, simulate it, and find a way to avoid it. Hartwell and Gehrke [12] reported the presence of alpha emitting nuclides in $LaCl_3$:Ce and identified the contamination as ^{227}Ac and its daughters. Milbrath et al. [13] characterized an alpha contamination in $LaCl_3$:Ce with coincidence measurements and provided further evidence of ^{227}Ac presence. Later, Quarati et al. [14] studied radioactive decays of ^{138}La in $LaBr_3$:Ce and measured the shape of the internal β spectrum. These data were used later by Camp et el. [15] to successfully simulate an internal β and gamma spectrum from ^{138}La with PENELOPE/penEasy Monte Carlo code. Quarati et al. [1] also studied an alpha contamination in $CeBr_3$ and $LaBr_3$:Ce.

Despite these efforts, the shape of the internal alpha spectrum in lanthanide-based scintillators is still not fully understood. An attempt to simulate an internal alpha spectrum was not completely successful

* Corresponding author.
E-mail address: w.w.wolszczak@tudelft.nl (W. Wolszczak).

http://dx.doi.org/10.1016/j.nima.2017.02.041
Received 20 December 2016; Received in revised form 10 February 2017; Accepted 13 February 2017
Available online 20 February 2017

in $LaBr_3$:Ce [16], while recently Mesick et al. [2] simulated an alpha spectrum very accurately in CLLB. If an alpha activity in both scintillators is caused by the same ^{227}Ac contamination, then why does an alpha spectrum shape depend on a host material (compare [1,3,13])?

The aim of this study is to provide a deeper understanding of an internal α spectrum in the following lanthanide-based scintillators: $CeBr_3$, $LaBr_3$:Ce and $LaBr_3$:Ce,Sr (5% of Ce, 500 ppm of Sr). In Section 2 of this article, we discuss the origin of an intrinsic contamination in lanthanide-based scintillators in order to clarify which isotopes and alpha decays are expected in an internal background spectrum. Next, by analyzing the experimental data of Milbrath et al. [13] we show the influence of nuclear de-excitations on positions of internal alpha peaks. In Section 4, we calculate the time evolution of ^{227}Ac and its daughters with Bateman equations, which provides an understanding of the relative intensities of alpha peaks. Then, we present measurements of the background spectrum of the three mentioned materials performed with modern digital techniques. The results prove the usefulness of pulse shape discrimination (PSD) for separating α from γ events, and a time-amplitude analysis for selecting ^{219}Rn and ^{215}Po decays from a total α spectrum. Our results explain why the previous attempt to simulate an α spectrum in $LaBr_3$:Ce [16] was not successful. Finally, we compare our experimental results with a GEAN4 simulation to verify the role of nuclear gamma de-excitations in shaping an internal alpha spectrum.

2. Origin of intrinsic contamination

The decay chain of ^{227}Ac is a sub-chain of the uranium 235 series (also called the "4n+3 chain"). The most probable path of ^{227}Ac decay goes through the following isotopes (see Fig.1): $^{227}_{89}$Ac → $^{227}_{90}$Th → $^{223}_{88}$Ra → $^{219}_{86}$Rn → $^{215}_{84}$Po → $^{211}_{82}$Pb → $^{211}_{83}$Bi → $^{207}_{81}$Tl → $^{207}_{82}$Pb and ends on a stable lead-207. In this chain there are five α decays and three β^-. Since ^{227}Ac has the longest decay time, the rate of consequent decays is limited by that of actinium, and equal rate for all following daughter's decays may be expected (this will be discussed in detail in Section 4). On the other hand, in measurements of an intrinsic α particle background in ^{227}Ac contaminated crystals, we observe three broad bands, instead of five equal intensity α peaks. Shoulders or an additional low intensity peak are observed in some measurements, which makes an internal alpha spectrum difficult to analyze. Fig. 2 shows an exemplary spectrum of an intrinsic activity pulse height spectrum (PHS) measured in a commercial $LaBr_3$:Ce scintillator (BrilLance380™). A similar structure was reported for $LaCl_3$:Ce [10] and $CeBr_3$ [1]. On the right side of the picture we see a broad structure of three main peaks, ascribed to α particle detection, and a small satellite peak between the 2nd and 3rd main peaks. These peaks do not have the same intensity (height) as one would expect: the first and the second peak are equally intense, the satellite peak is two times less intense, and the third peak is the least intense.

3. Coincidence measurement analysis

Not only does the α energy spectrum have missing peaks, but identifying corresponding isotopes and α energies is also problematic.

Quarati et al. [1] analyzed the $LaBr_3$:Ce internal contamination spectrum and identified the peaks as follows: the first peak in the structure (see Fig. 2) as ^{223}Ra (E_α=5716 keV), no peak from ^{227}Th, the second peak as ^{211}Bi (E_α=6623 keV), the satellite peak as ^{219}Rn (E_α=6819 keV), and the third peak as ^{215}Po (E_α=7386 keV). However, the values of the α/β ratio calculated with these energies are inconsistent (namely: 0.359, 0.343, 0.348, 0.359). The three last values increase with the energy, but the first one is exceptionally high. Recent research showed that the α/β ratio increases monotonically, approximately linear, with α energy in many scintillators at alpha

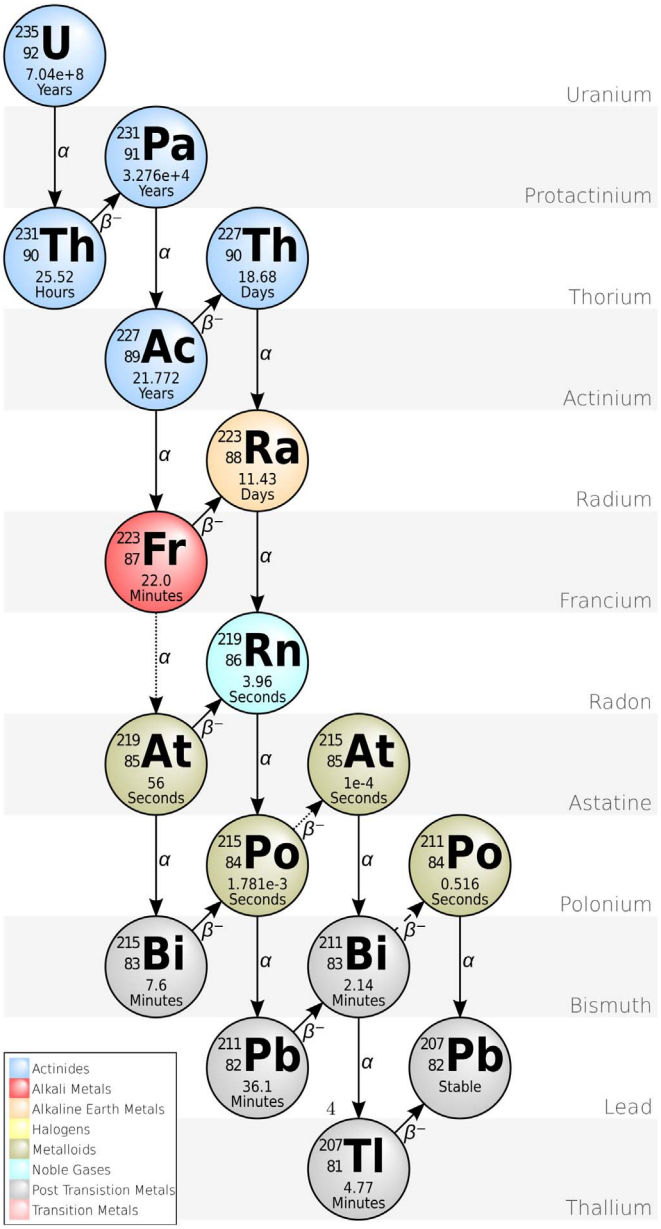

Fig. 1. $^{235}_{92}$U decay chain: actinium series. Dashed arrow is a decay mode with <1% probability. Dotted arrows are decay modes with <0.01% probability. Graphics by Edgar Bonet used under CC BY-SA 3.0 license.

energies higher than 2 MeV (a review on the α/β will be published separately [17]). This suggests that the identification of the first peak as ^{223}Ra needs to be reconsidered.

Hartwell et al. [9] identified the first peak as a mixed peak of ^{223}Ra and ^{227}Th, but in the analysis of the alpha response linearity they used the energy of ^{227}Th (~6 MeV), which resulted in a linear relation of the α/β ratio on the alpha energy. On the other hand, Negm et al. [16] have ascribed the first peak to ^{223}Ra E_α=5716 keV, which again resulted in a deviation from the linear relation between the α/β ratio and E_α.

To solve these inconsistencies we analyzed coincidence measurements done by Milbrath et al. for $LaCl_3$:Ce [8], but we found another complication for the α spectrum analysis. Milbrath et al. performed a measurement of the $LaCl_3$:Ce internal alpha spectrum in coincidence with gamma escapes detected by a High Purity Germanium (HPGe) detector. They looked for alpha decays followed by immediate gamma de-excitation and escape from the crystal. The same alpha particle energy was expected in coincidence with multiple γ energies, but in fact the measured alpha energies were also different. For instance, ^{227}Th

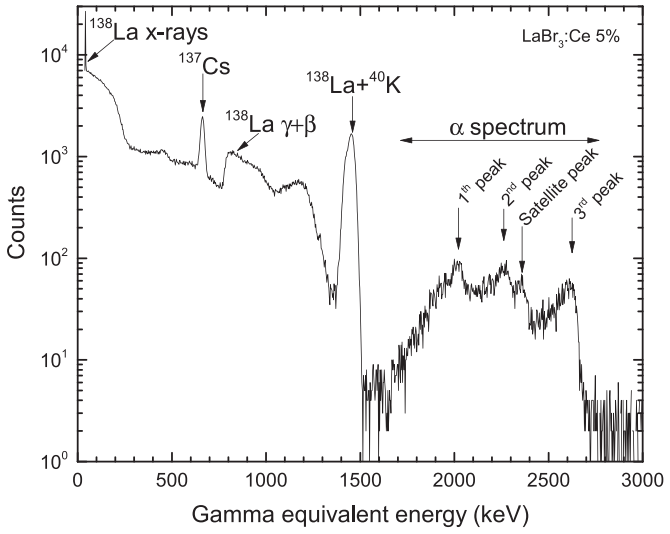

Fig. 2. Exemplary intrinsic activity spectra of 1 in. $LaBr_3$:Ce (5 mol% of cerium). ^{137}Cs source was placed for energy reference.

decays with 5757 keV α emission and can be followed either by 236.0 keV, 256.3 keV or 286.1 keV γ (see Table 1 in [8]). Nevertheless, the α energies measured in coincidence were the following: 5831 keV, 5781 keV and 5727 keV. This means that for the same true α particle energy three different energies were actually measured. The difference exceeds the standard deviation which ranged from 44 to 65 keV. If one calculates the α/β ratio,[1] the values for 5757 keV α energy are 0.324, 0.320 and 0.316, which is a non-physical result.

We can investigate this by taking a closer look at the simplified ^{227}Th decay scheme shown in Fig. 3. After the α decay with E_α=5757 keV the daughter nucleus is in the excited state at 286.1 keV energy. It can de-excite by three different ways from this state:

- by emitting a single 286 keV γ photon,
- by emitting 256 keV and 50.1 keV γ photons, or
- by emitting 226 keV and 29.8 keV γ photons.

The lifetime of the ^{227}Th excited nuclear state is very short (shorter than 1 ns), so the gamma particle will be absorbed in a crystal and measured together with the alpha particle as a single event (shaping time used for collecting the scintillator signal is usually much longer than hundreds of ns). In case of 236 keV γ escape there is a high probability that a 50.1 keV gamma will be absorbed in a crystal and recorded together with the 5757 keV α. Because a γ photon has much higher light yield (per MeV) than an α particle, a significant amount of light will be added to an alpha event.

If one removes the energy of the second photon from an alpha event, then the α/β curve significantly improves when compared to the raw data. Fig. 4 shows the α/β ratio of $LaCl_3$:Ce calculated with raw Milbrath data [13] and the α/β ratio refined by subtracting the gamma energy. Deviation of the α/β ratio curve from linearity significantly decreases when the scintillation light added by gamma de-excitations is subtracted.

From the above analysis we can conclude that alpha decays followed by gamma nuclear de-excitations will be measured with a scintillator at higher energies than that of the alpha particle alone. Such an effect is not observed with typical α particle detectors (e.g., silicon surface barrier detectors), because they are not sensitive to gamma

[1] α/β ratios were obtained by calculating measured α energies from Table 1 in [8] to γ-equivalent energy scale using equation $AlphaEnergy = (GammaEnergy) \times 2.2784 + 1578.6$ (in units of keV) and dividing by a true α particle energy.

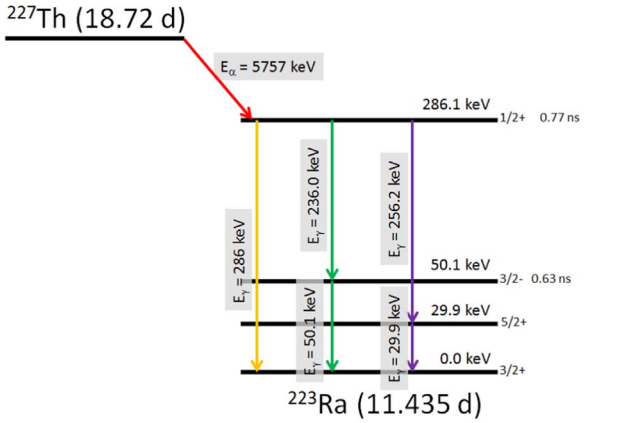

Fig. 3. Simplified nuclear levels chart of ^{227}Th isotope decaying into ^{223}Ra by 5757 keV α emission. Other possible α decay modes, excited nuclear levels of ^{223}Ra and low intensity/forbidden γ transitions were excluded for clarity.

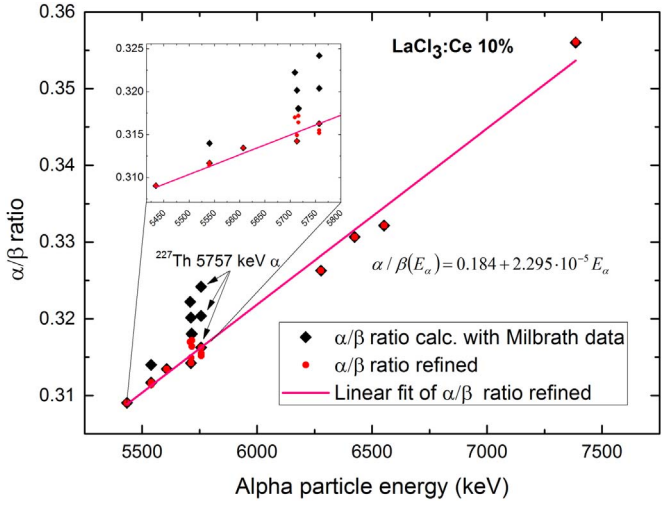

Fig. 4. α/β ratio of $LaCl_3$:Ce 10 mol% calculated using Milbrath coincidence data [8] in function of true α particle energy (black diamonds) compared with α/β ratio calculated with subtracting γ photon energy left in scintillator (refined data, red circles). The inset shows energy range of ^{227}Th and ^{223}Ra isotopes for which multiple coincidences for the same true α energy were observed. (For interpretation of the references to color in this figure legend, the reader is referred to the web version of this article.)

photons, and they measure an alpha particle energy alone. To understand the shape of an internal contamination α spectrum we need to take into account all electromagnetic processes following a nuclear decay: γ de-excitations, Compton effect, Auger electron emission, and X-ray fluorescence.

4. Time evolution of ^{227}Ac contamination

To investigate alpha peak intensities in an internal contamination spectrum, we first analyzed the time evolution of concentrations and activities of the ^{227}Ac isotope and its daughters. The differential equations governing successive radioactive decays can be written as

$$\begin{aligned}\frac{dN_1(t)}{dt} &= -\lambda_1 N_1(t),\\ \frac{dN_2(t)}{dt} &= -\lambda_2 N_2(t) + \lambda_{1,2} N_1(t), \ldots\\ \frac{dN_n(t)}{dt} &= -\lambda_n N_n(t) + \lambda_{n-1,n} N_{n-1}(t),\end{aligned} \quad (1)$$

where $N_i(t)$ is a number of atoms of a radioisotope i at a time t, λ_n is a total removal decay constant (including all decay branches), $\lambda_{i-1,i}$ is a partial decay constant (related to single decay branch from isotope

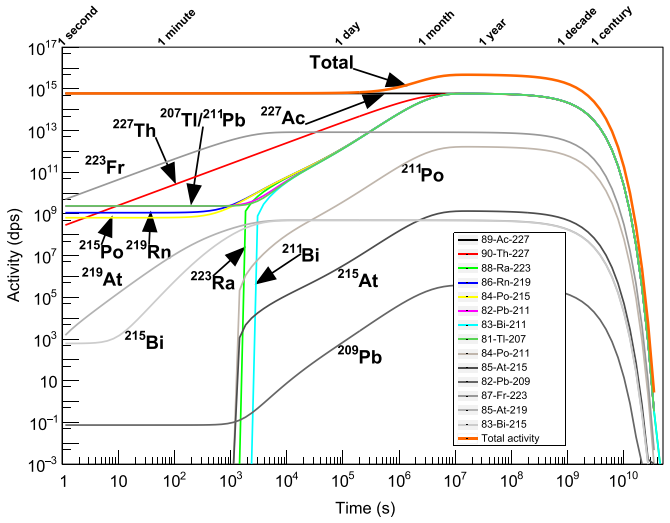

Fig. 5. Evolution of activities of ^{227}Ac isotope and it's daughters starting from 1 mol of pure ^{227}Ac. Activities are expressed in decays per second (dps), including all possible decay branches of a particular isotope. Orange line shows the sum off all decay rates in the sample (For interpretation of the references to color in this figure legend, the reader is referred to the web version of this article.)

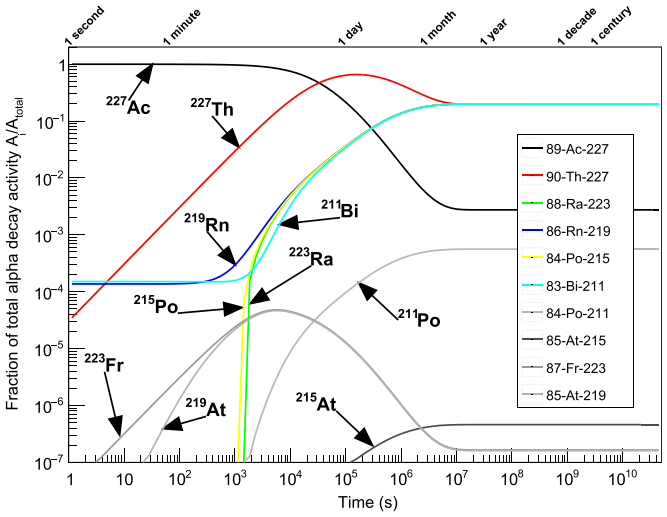

Fig. 6. Time evolution of fractions of total alpha activity of ^{227}Ac isotope and it's daughters starting from 1 mol of pure ^{227}Ac.

$i-1$ to i) calculated from a branching ratio $\lambda_{i-1,i} = b_{i-1,i}\cdot\lambda_{i-1}$. The solution of this set of equations was first proposed by Bateman [18] for the case without a decay chain branching. The general problem solution, with included decay chain branching, was proposed by Skrable [19] as follows:

$$N_i(t) = N_1(0)\prod_{j=1}^{i-1}\lambda_{j,j+1}\times\sum_{j=1}^{i}\frac{e^{-\lambda_j t}}{\prod_{\substack{p=1\\ p\neq j}}^{i}(\lambda_p-\lambda_j)}. \quad (2)$$

To calculate the solutions, we used TGeo package from the ROOT framework [20]. The calculations were performed assuming one mole of pure ^{227}Ac at the beginning, evaluated during 10^{11} s. There are 16 isotopes involved in the entire ^{227}Ac decay chain, which starts with ^{227}Ac and ends on stable $^{207}_{82}$Pb, accompanied by a small amount ($\sim 10^{14}$ atoms) of stable $^{209}_{83}$Bi produced through a cluster decay: $^{223}_{88}\mathrm{Ra} \rightarrow {}^{209}_{83}\mathrm{Bi} + {}^{14}_{6}\mathrm{C}$.

Eq. (2) provides a solution for the number of atoms as a function of time. Since the number of atoms is not easily measurable, we are rather interested in activities. In Fig. 5 we show the calculated decay rates of the isotopes, according to the formula $A_i = N_i\lambda_i$, where λ_i is a decay constant of isotope i. Activities are expressed in the number of disintegrations per second, so they include all possible decay channels of a particular isotope. From this plot one can see that the total activity $A_{total} = \sum A_i$ increases first, and after reaching an equilibrium stage at day 109 it decreases exponentially, being limited by the ^{227}Ac decay rate. The important fact is that ^{227}Ac, ^{227}Th, ^{223}Ra, ^{219}Rn, ^{215}Po, ^{211}Pb and ^{207}Tl all have the same decay rate after reaching the equilibrium state.

Fig. 5 shows the decay rates of the isotopes. However, we are interested in alpha decay rates specifically, since they correspond to the intensities of the alpha peaks in the internal background spectrum. For instance, in case of the ^{227}Ac alpha decay, the branching ratio α-BR(^{227}Ac) =1.38% is very low. Consequently, the ^{227}Ac alpha peak intensity is almost a hundred times lower than the alpha peaks of ^{227}Th or ^{223}Ra, even though all three have the same decay rate. The amount of the initial contamination of ^{227}Ac is usually unknown, so from a practical point of view a ratio of an alpha decay rate to the total alpha activity is more useful than just an absolute activity. Fig. 6 shows the ratio of alpha isotopes decay activity A_i (multiplied by the α branching ratio) to the total activity A_{total} of all alpha decaying isotopes. During the first 8 h, the alpha decays are dominated by decays of ^{227}Ac, then alpha activity from ^{227}Th increases. Finally, after 109 days the decays of ^{227}Th, ^{223}Ra, ^{219}Rn, ^{211}Bi and ^{215}Po reach equal decay rates, while the activity of ^{227}Ac decreases and becomes more than two orders of magnitude lower then others. The alpha activities of ^{211}Po, ^{215}At, ^{223}Fr and ^{219}At isotopes are many order of magnitude lower, so these isotopes are extremely difficult to detect on a statistically significant level.

The main conclusion is that after 109 days the decaying isotopes are in equilibrium and activities of alpha decays of ^{227}Th, ^{223}Ra, ^{219}Rn, ^{211}Bi, and ^{215}Po are equal. Very low activity from ^{227}Ac alpha decays may be also detected, and in fact a weak ^{227}Ac alpha peak was reported by Hartwell et al. [9].

5. Materials and methods

5.1. Samples and experimental setup

The intrinsic activities of the following three samples were measured: a 3 by 3 in. cylinder of $LaBr_3$:Ce (5 mol% of Ce), a 2 by 2 in. cylinder of $CeBr_3$ and a bare sample of approximately 10 mm×5 mm×20 mm $LaBr_3$:Ce,Sr (5 mol% of Ce, <0.5 mol% of Sr). The first two samples were encapsulated by the manufacturer, Saint Gobain Corporation, and the third sample was encapsulated in our lab into a hermetic can with a quartz window.

Fig. 7 shows the schematic of the experimental setup. A measured sample was coupled with an optical grease to an XP4312 photomultiplier tube (PMT) and placed inside a light-proof casing. A laser diode was mounted in the casing pointing to the photocathode of the PMT. The laser light pulses were used in the later data analysis for a gain correction. The casing was put in a 15 cm thick lead castle in order to reduce natural background in the measurement. The raw signal from the 50 Ω terminated anode was directly connected to the 50 Ω input of a CAEN Digitizer model 5730.

5.2. Data acquisition and analysis

The digitizer generates an internal trigger when an input signal exceeds the threshold voltage V_{th}. The input signal is sampled with 14-bit precision and 500 Mega Samples per Second (MSPS) sampling rate and stored in a buffer. Each stored waveform has 1280 samples (2560 ns) and is attached with a 32 bit counter of the Trigger Time Tag (TTT). The time resolution of TTT is 12 ns.

Home made data acquisition software (DAQ) was developed for controlling data acquisition, data transfer to a PC, performing an initial analysis, and storing the results in ROOT data file format [20]. Since the TTT counter overflows after around 17 s, every buffer received from the digitizer was attached by the DAQ with a local PC Time Tag (PTT).

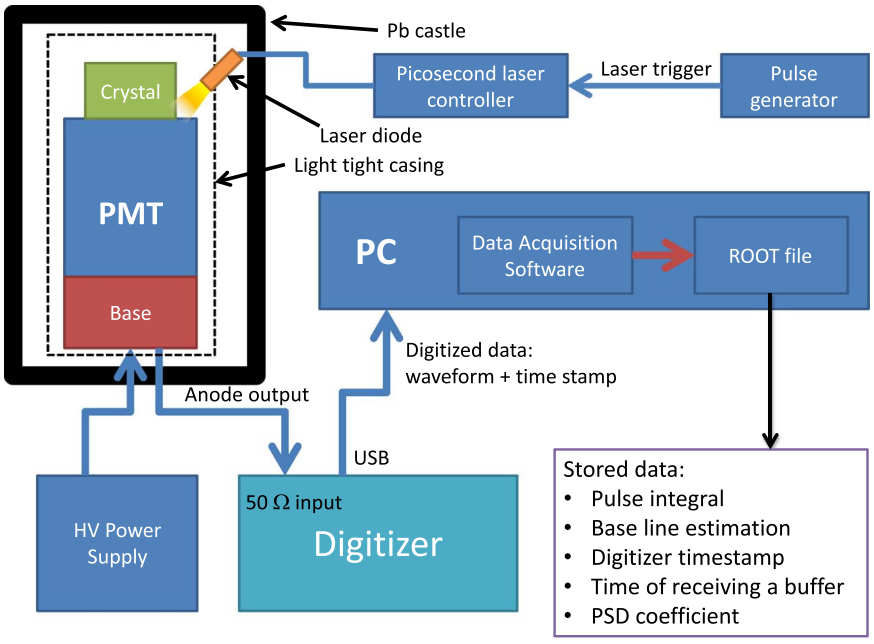

Fig. 7. Schematic of the digital nuclear spectroscopy setup.

The PTT was used in a later analysis for time ranges exceeding the TTT counter size.

Fig. 8 shows the steps of the data analysis. The three first steps are calculated for every event during a data acquisition: a base line V_{BL}, a pulse integral Q_{total}, and a pulse shape discrimination (PSD) factor V_p/Q_{total}. The base line V_{BL} is calculated as an arithmetic average of the first 340 samples, when a scintillation pulse is not yet present. The pulse integral is calculated by subtracting the base line V_{BL} from the waveform and summing values of 150 samples (300 ns) starting from the end of the base line calculation window. The integration time of 300 ns is sufficient for the fast cerium scintillators studied in this work. For Pulse Shape Discrimination (PSD), a PSD factor V_p/Q_{total} as described by Ogawara et al. [21] was calculated as a ratio of a raw pulse maximum amplitude V_p to integrated charge Q_{total}.

Fig. 9 shows an exemplary plot of a PSD factor versus a gamma equivalent energy measured with a 1 in. $LaBr_3$:Ce sample exposed to ambient radiation. The band centered around $V_p/Q_{total} \approx 0.07$ displayed across all energies and widening toward lower energy comes from gamma/electron events, while a small band in the energy range 1.7–2.7 MeV, with slightly higher V_p/Q_{total}, is caused by alpha particle events. One may notice a gamma peak from $^{40}K/^{138}La$ events around 1.5 MeV and a weak gamma peak from ^{208}Tl around 2.6 MeV. An alpha particle window was accordingly adjusted for selection of alpha events in different samples. The example plot shows the importance of usage of PSD in this case, since the ^{208}Tl γ-peak overlaps with the alpha spectrum and without that technique it is difficult to distinguish gamma decays from ^{208}Tl and alpha decays from ^{215}Po.

5.3. Time-amplitude analysis

We used features of the ^{226}Ac decay chain in the off-line analyses to select only a specific sequence of events in an energy-time space. Since ^{219}Rn decays into ^{215}Po with decay time of around 4 s, and ^{215}Po decays to ^{211}Pb with decay time around 1.8 ms (see Fig. 1), in off-line analysis we selected pairs of alpha decays falling within the 20 ms coincidence window. Additionally, we added energy criteria by requiring that the first event has the energy of a ^{219}Rn alpha decay, and the second that of a ^{215}Po decay: ^{219}Rn ($T_{1/2} = 3.98$ s, $Q_\alpha = 6946$ keV)→^{215}Po ($T_{1/2} = 1.781$ ms, $Q_\alpha = 7526$ keV). This eliminated most random events and filtered out only Rn-Po event pairs.

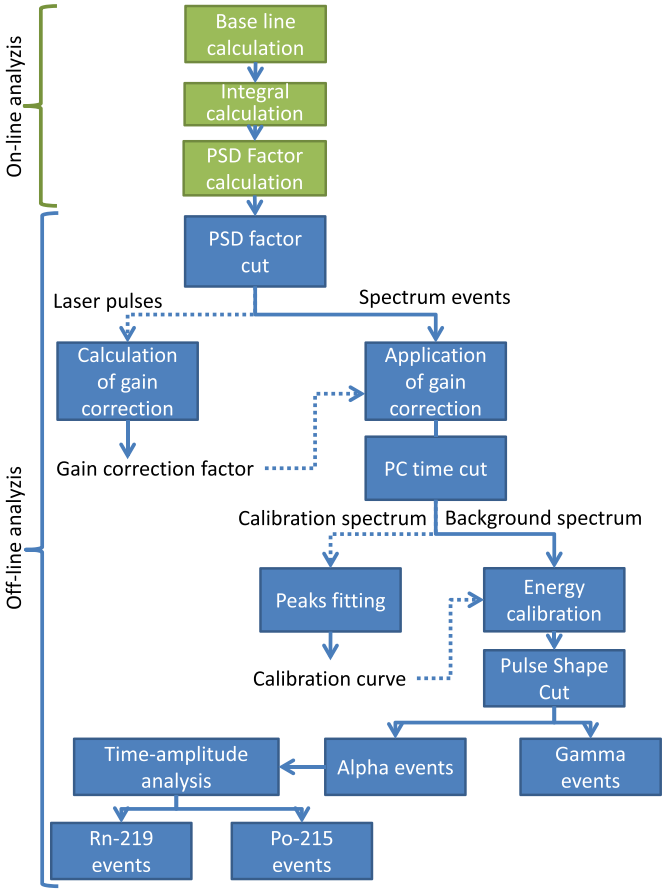

Fig. 8. Steps of the data analysis.

5.4. Simulation

In order to verify the importance of the gamma de-excitations we simulated the internal alpha spectrum in $LaBr_3$:Ce,Sr with the Geant4 toolkit and home made analysis software. Decays of ^{223}Ra, ^{227}Th, ^{211}Bi,

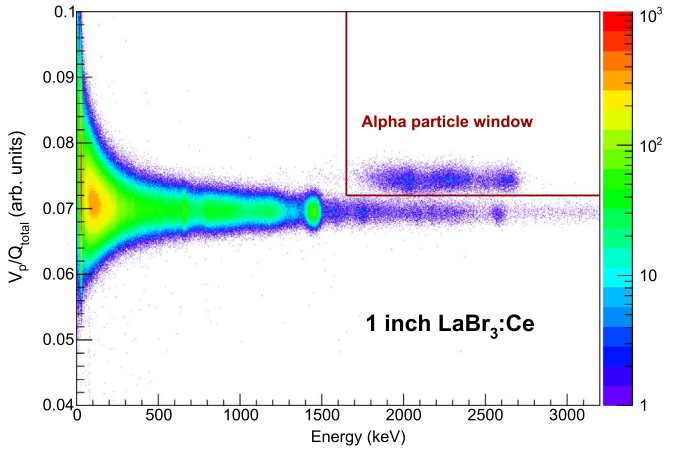

Fig. 9. Pulse shape discrimination parameter V_p/Q_{total} in function of γ-equivalent energy measured with ϕ1 in.×1 in. $LaBr_3$:Ce crystal, exposed to ambient radiation. Colour represents the number of counts. Internal alpha decays are easily distinguishable from a gamma background. (For interpretation of the references to color in this figure legend, the reader is referred to the web version of this article.)

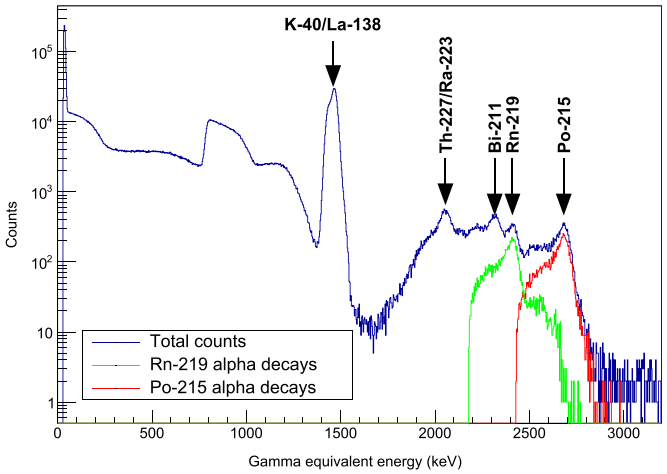

Fig. 10. Intrinsic activity energy spectrum (dark blue) measured with 3 in. $LaBr_3$:Ce (5 mol% of Ce) crystal together with Radon-219 (green) and Polonium-215 (red) peaks separated using amplitude-time analysis. (For interpretation of the references to color in this figure legend, the reader is referred to the web version of this article.)

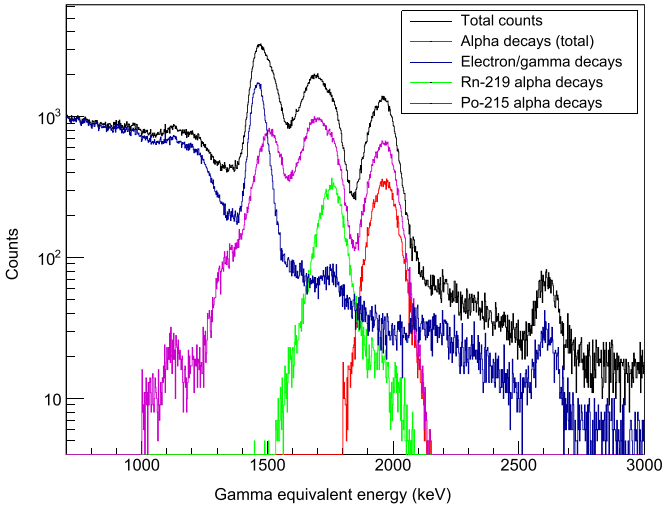

Fig. 11. Intrinsic activity energy spectrum measured with 2 in. $CeBr_3$ crystal. Alpha (magenta) and gamma events (dark blue) were separated with PSD, then Radon-219 (green) and Polonium-215 (red) peaks were separated using time-amplitude analysis. (For interpretation of the references to color in this figure legend, the reader is referred to the web version of this article.)

^{219}Rn, ^{215}Po in equal amounts were simulated including α decays, internal conversion and Auger de-excitations. The observed energy E'_m in particular event m was calculated by including the α/β ratio of the α particle, and the gamma Y_γ and an electron nonproportionality Y_e, according to the following formula:

$$E'_m = E_\alpha \cdot \alpha/\beta(E_\alpha) + \sum_{i=1}^{n_e} E_e \cdot Y_e(E_e) + \sum_{i=1}^{n_\gamma} E_\gamma \cdot Y_\gamma(E_\gamma). \quad (3)$$

E_α, E_e, E_γ are true energies of the α, electrons and gammas in m event; summing goes over all electrons n_e and gammas n_γ in the event. We used electron nonproportionality data Y_e and gamma non proportionality Y_γ from [22].

We did not find appropriate data on the α/β ratio as a function of alpha energy, so we used a linear model as approximation (see also Fig. 4)

$$\alpha/\beta(E_\alpha) = a + b \cdot E_\alpha, \quad (4)$$

where a and b are free parameters fitted to the experimental data. Comprehensive justification of the linear approximation will be presented in a separate article on the α/β ratio [17].

The energy resolution was simulated by convoluting the generated spectrum with an energy resolution model $R(E') = A\sqrt{E'}$, where A is a free parameter and E' is an observed (quenched) energy.

6. Results

6.1. Measurement

Figs. 10–12 show the internal background spectra of the measured samples: $LaBr_3$:Ce, $CeBr_3$ and $LaBr_3$:Ce,Sr respectively. The main feature for all three samples is a peak located around 1450 keV which originates from potassium ^{40}K gamma decays and/or ^{138}La decay daughter de-excitation in the case of $LaBr_3$. In $LaBr_3$:Ce and $LaBr_3$:Ce,Sr this peak appears at a lower channel number than the measured alpha spectrum, but in the case of $CeBr_3$:Ce it overlaps with it. Hence, a suppression of the potassium presence or PSD becomes crucial for measuring a pure alpha spectrum in $CeBr_3$.

Alpha events were separated from electron/gamma events by using PSD (see Fig. 9). Peaks originating from ^{219}Rn and ^{215}Po alpha decays were separated from the rest of the alpha decays with time-amplitude analysis. In Figs. 10–12 alpha particle spectra with separated peaks are shown for $LaBr_3$:Ce, $CeBr_3$:Ce and $LaBr_3$:Ce,Sr samples. The main difference between the samples is the position of the alpha spectrum on a gamma calibrated energy scale. Since the true energies of alpha decaying isotopes are the same, it means that the alpha particle light yield quenching is significantly different in these materials. The quenching is the lowest in $LaBr_3$:Ce,Sr and the highest in $CeBr_3$:Ce.

Note that an asymmetric shape of the alpha peaks is observed for $LaBr_3$:Ce (Fig. 10) and $LaBr_3$:Ce,Sr (Fig. 12), but not for $CeBr_3$ (Fig. 11). Fig. 13 shows the alpha peaks from ^{219}Rn and ^{215}Po isotopes in $LaBr_3$:Ce,Sr with a double-Gaussian fit used as a model. This model is used for mathematical simplicity, without physical justification. Consequently, the energy resolutions shown in Fig. 13 should not be treated as precise and quantitative.

Table 1 lists the α/β ratio measured with an internal alpha activity and analyzed with the time-amplitude analyses. In case of asymmetric alpha peaks in $LaBr_3$:Ce and $LaBr_3$:Ce,Sr the highest intensity peak was used for calculating the α/β ratio. As one can notice, the α/β ratio increases from $CeBr_3$, $LaBr_3$:Ce up to $LaBr_3$:Ce,Sr. Furthermore, the α/β ratio increases with the true alpha energy for all studied materials.

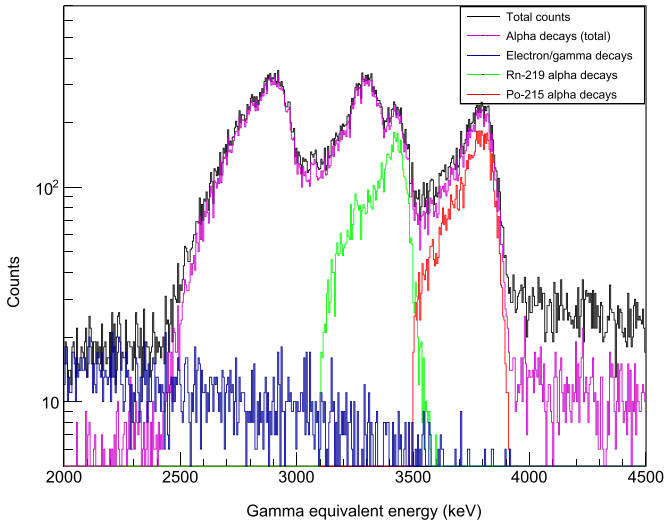

Fig. 12. Internal background spectrum of $LaBr_3$:Ce, Sr sample with alpha and electron/gamma events separated. Alpha peaks from ^{215}Po and ^{219}Rn were separated from total alpha decays spectrum with time-amplitude method. Gamma/electron background is clean from any peaks at energy range where alpha particles are observed (2400–4000 keV). From the alpha discriminated spectrum, it is clear that alpha peaks are asymmetric. (For interpretation of the references to color in this figure legend, the reader is referred to the web version of this article.)

6.2. Simulation

Fig. 14 compares the simulation (red curve) and the measurement (black curve) of the internal alpha background in $LaBr_3$:Ce,Sr. Separate energy spectra of the constituent isotopes are shown below the red curve, while the energies without including an energy resolution are shown as vertical lines. One may notice that ^{215}Po has a single vertical line corresponding to an α decay directly to the ground state of the daughter nucleus. The simulation successfully reproduces the main feature of the internal activity spectrum: the three band structure. However, a low energy tail is present for every band in the measured spectrum. It is especially visible for Ra/Th peak, which is followed by a

Table 1
α/β ratio measured in different materials using time-amplitude analysis to separate Po-215 and Rn-219 alpha peaks from α internal background.

Material	Isotope	True α energy (keV)	Measured γ equivalent (keV)	α/β ratio
$LaBr_3$:Ce,Sr	Po-215	7386.1	3804	0.515
$LaBr_3$:Ce,Sr	Rn-219	6819.2	3435	0.504
$LaBr_3$:Ce	Po-215	7386.1	2682	0.363
$LaBr_3$:Ce	Rn-219	6819.2	2410	0.353
$CeBr_3$	Po-215	7386.1	1966	0.266
$CeBr_3$	Rn-219	6819.2	1753	0.257

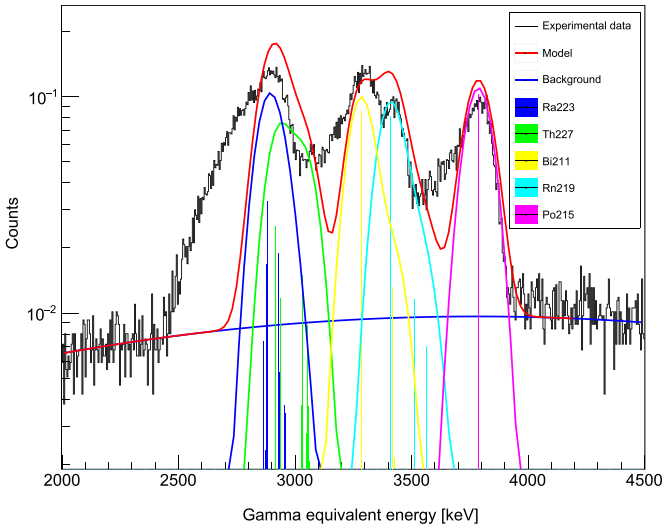

Fig. 14. Comparison of simulation of internal alpha activity (red curve) of Ac-227 and the measured data (black curve) with $LaBr_3$:Ce, Sr. The simulation includes all de-excitation processes (X-ray fluorescence, Auger electrons emission) and assumes complete absorption of all γ photons. (For interpretation of the references to color in this figure legend, the reader is referred to the web version of this article.)

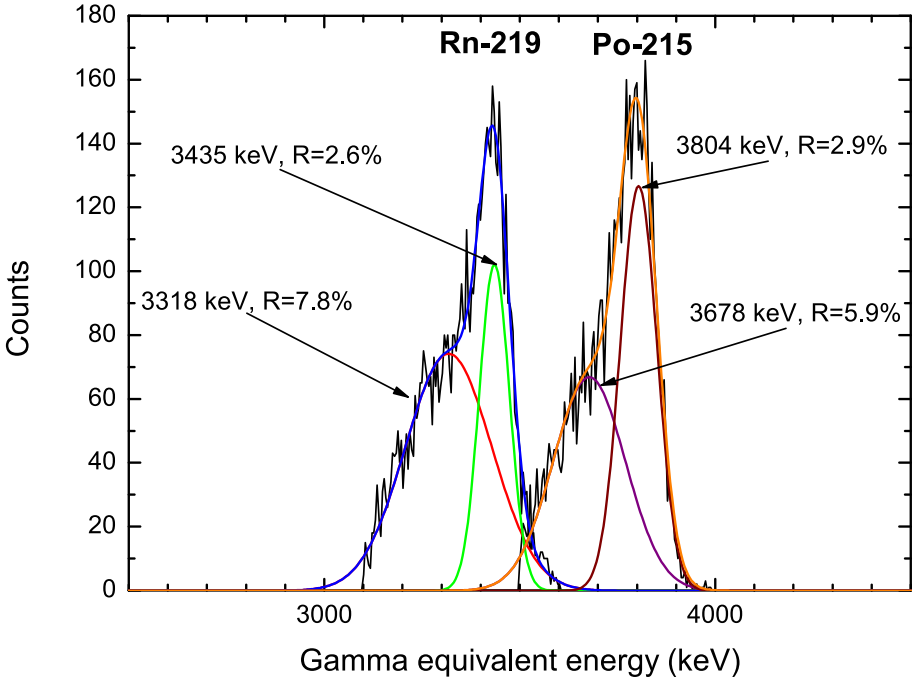

Fig. 13. Rn-219 and Po-215 alpha peaks measured with internal contamination background in $LaBr_3$:Ce, Sr sample and separated from total background spectrum using pulse shape discrimination and time-amplitude analysis. Asymmetry of alpha peaks is clearly visible.

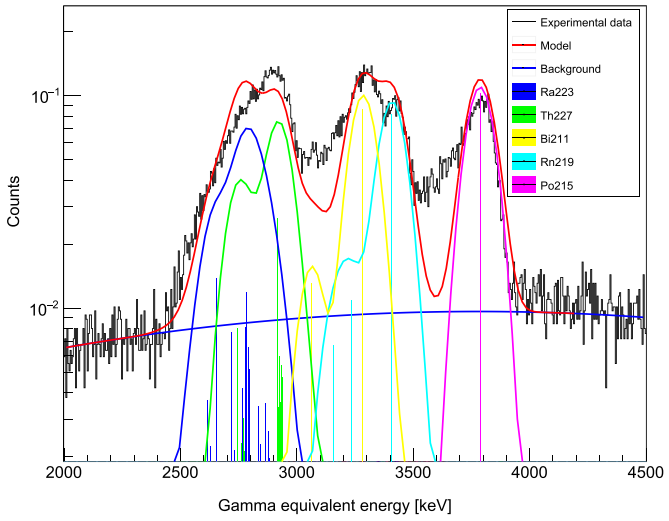

Fig. 15. Comparison of Ac-227 alpha activity simulation (red curve) and the measured data (black curve) with $LaBr_3$:Ce, Sr . The simulation assumes no contribution from gamma photons (all photons escape from the crystal). (For interpretation of the references to color in this figure legend, the reader is referred to the web version of this article.)

long tail on the left side. As a consequence it has a lower intensity than expected from the simulation. Similarly the peak-to-valley ratio between ^{219}Rn and ^{215}Po is lower due to events coming from the tails. The disagreement is anticipated, since the asymmetric shape of alpha peaks was not included in the simulation. This provides further evidence that the asymmetric shape previously shown in Fig. 13 is crucial for understanding the spectrum shape.

Fig. 15 shows the simulation of the internal alpha spectrum excluding the contribution of gamma photons, assuming that all gamma photons escape from the crystal without being absorbed (the third term in Eq. (3) is abandoned). In this case, the Ra/Th peak is a double peak, which is not observed in the measurement. The spectrum simulated in this way is very different from the measured with $CeBr_3$ (Fig. 11) and $LaBr_3$:Ce (Fig. 10).

One may compare the ^{219}Rn peak in Fig. 14 and the same peak in Fig. 15. The low intensity lines of mixed α/γ events are on the right side of the highest intensity line in the simulation which included gamma de-excitations (Fig. 14). In the second case, when the gamma absorptions were excluded (all gamma photons escape), the low intensity lines are on the left (Fig. 15). This proves that a correct simulation of an internal background spectrum in scintillators is impossible without taking into account gamma interactions. In fact, the shape of a measured spectrum is somewhere in between a complete gamma absorption simulation and a complete escape, additionally smeared by Compton scattering.

7. Discussion

In case of lanthanum-based scintillators, we observe asymmetric alpha peaks (see Figs. 13 and 10). In contrast, in $CeBr_3$, alpha peaks are symmetric (compare Fig. 11). The asymmetric peaks with low energy tails are responsible for a low valley-to-peak ratio observed in an internal background spectrum of $LaBr_3$:Ce, $LaBr_3$:Ce,Sr, and probably in $LaCl_3$:Ce [13]. The origin of this phenomenon is unknown. We considered several hypotheses to explain the effect, and we concluded that the most probable is the presence of light yield non-uniformities in the crystal structure. These non-uniformities can exist on the length scale of the α particle track length (~25 μm) and are washed out with much longer β-tracks.

We excluded the role of X-ray or gamma escape in that process by analyzing coincidence measurements done by Milbrath [13]. From Fig. 13 one can see that energy difference between “main” peaks and “escape” peaks is around 100 keV, but such energies were not observed in a coincidence with ^{219}Rn and ^{215}Po peaks.

The simulation (Fig. 14) shows that ^{215}Po decays with emission of a single α energy, so it is not disturbed by gamma absorption. On the other hand, the ^{219}Rn alpha peak can be recorded with accompanying gamma de-excitations, which can be seen in Fig. 14 as a tail at the high energy side of the peak. The tail is caused by recording an α particle with de-excitation gamma photon. As gamma photons have higher light yield then alpha particles, the lines are seen on the right side from the main alpha peak. The reader may compare the simulated ^{219}Rn peak shape with the peaks measured with time-amplitude analysis in $LaBr_3$:Ce (Fig. 10) and $CeBr_3$ (Fig. 11).

In the simulation we assumed that all gamma photons are absorbed within the scintillator. This assumption is justified for big crystals, like 2 in. $CeBr_3$ (Fig. 10) and Fig. 3 inch $LaBr_3$:Ce (Fig. 11), but does not hold for the small sample of $LaBr_3$:Ce,Sr (Fig. 12). A high energy tail made of α-γ mixed events is visible in 3 in. $LaBr_3$:Ce and 2 in. $CeBr_3$, but it disappears in the small $LaBr_3$:Ce,Sr sample (Fig. 12).

8. Conclusions

Digital spectroscopy can be a powerful tool for studying scintillators, and it makes possible to perform a complex analysis like a pulse shape discrimination or a time-amplitude analysis. This permitted us to investigate the complex structure of an internal alpha spectrum in $LaBr_3$:Ce, $LaBr_3$:Ce,Sr and $CeBr_3$.

An alpha spectrum measured in a scintillator with an internal contamination can be significantly distorted by gamma de-excitations of decay products. This is because an alpha particle can be detected together with a gamma photon as a single event, but both particles have significantly different light yields. This conclusion is particularly important for everyone trying to simulate an internal alpha activity. In addition, measuring the α/β ratio with an internal alpha contamination seems to be an attractive way of avoiding surface effects, but it can not be easily done with an alpha isotope decaying into an excited state of a daughter nucleus.

By applying time-amplitude cuts on the acquired data, we were able to separate Po-215 and Rn-219 alpha peaks from the total spectrum. By this means, we found asymmetric alpha peaks in $LaBr_3$:Ce and $LaBr_3$:Ce,Sr but not in $CeBr_3$. The cause of this phenomenon is not known.

Our approach to include nuclear de-excitation processes in simulation is promising, and together with experimental data on asymmetric α peaks gives a way to construct a complete and accurate simulation of a scintillation response to an internal activity. We advise using the ^{215}Po alpha peak in future α/β ratio measurements, as this peak is made out of pure alpha decays to a ground state, not followed by any other type of de-excitation.

Acknowledgments

This work was supported by the Dutch Technology Foundation STW, which is part of the Netherlands Organization for Scientific Research (NWO), which is partly funded by the Ministry of Economic Affairs. This work was partly funded by Saint Gobain Crystals, France.

References

[1] F. Quarati, P. Dorenbos, J. van der Biezen, A. Owens, M. Selle, L. Parthier, P. Schotanus, Scintillation and detection characteristics of high-sensitivity $CeBr_3$ gamma-ray spectrometers, Nucl. Instrum. Methods Phys. Res. Sect. A: Accel. Spectrom. Detect. Assoc. Equip. 729 (2013) 596–604.

[2] K. Mesick, D. Coupland, L. Stonehill, Pulse-shape discrimination and energy quenching of alpha particles in $Cs_2LiLaBr_6:Ce^{3+}$, Nucl. Instrum. Methods Phys. Res. Sect. A: Accel. Spectrom. Detect. Assoc. Equip. 841 (2017) 139–143.

[3] R.S. Woolf, B.F. Phlips, E.A. Wulf, Characterization of the internal background for

thermal and fast neutron detection with {CLLB}, Nucl. Instrum. Methods Phys. Res. Sect. A: Accel. Spectrom. Detect. Assoc. Equip. 838 (2016) 147–153.
[4] R. Bernabei, P. Belli, A. Bussolotti, F. Cappella, R. Cerulli, C. Dai, A. dAngelo, H. He, A. Incicchitti, H. Kuang, J. Ma, A. Mattei, F. Montecchia, F. Nozzoli, D. Prosperi, X. Sheng, Z. Ye, The DAMA/LIBRA apparatus, Nucl. Instrum. Methods Phys. Res. Sect. A: Accel. Spectrom. Detect. Assoc. Equip. 592 (3) (2008) 297–315.
[5] W. Drozdowski, P. Dorenbos, A.J.J. Bos, G. Bizarri, A. Owens, F.G.A. Quarati, $CeBr_3$ scintillator development for possible use in space missions, IEEE Trans. Nucl. Sci. 55 (2008) 1391–1396.
[6] F. Danevich, V. Kobychev, O. Ponkratenko, V. Tretyak, Y. Zdesenko, Quest for double beta decay of ^{160}Gd and Ce isotopes, Nucl. Phys. A 694 (1) (2001) 375–391.
[7] F. Danevich, V. Kobychev, S. Nagorny, V. Tretyak, YAG:Nd crystals as possible detector to search for and decay of neodymium, Nucl. Instrum. Methods Phys. Res. Sect. A: Accel. Spectrom. Detect. Assoc. Equip. 541 (3) (2005) 583–589.
[8] B. Milbrath, R. Runkle, T. Hossbach, W. Kaye, E. Lepel, B. McDonald, L. Smith, Characterization of alpha contamination in lanthanum trichloride scintillators using coincidence measurements, Nucl. Instrum. Methods Phys. Res. Sect. A: Accel. Spectrom. Detect. Assoc. Equip. 547 (23) (2005) 504–510.
[9] J. Hartwell, R. Gehrke, Observations on the background spectra of four $LaCl_3$(Ce) scintillation detectors, Appl. Radiat. Isot. 63 (2) (2005) 223–228.
[10] B. Milbrath, J. McIntyre, R. Runkle, L. Smith, Contamination studies of $LaCl_3$:Ce scintillators, IEEE Trans. Nucl. Sci. 53 (2006) 3031–3034.
[11] J. Meija, T.B. Coplen, M. Berglund, W.A. Brand, P. De Bièvre, M. Gröning, N.E. Holden, J. Irrgeher, R.D. Loss, T. Walczyk, et al., Isotopic compositions of the elements 2013 (iupac technical report), Pure Appl. Chem. 88 (3) (2016) 293–306.
[12] J. Hartwell, R. Gehrke, Observations on the background spectra of four $LaCl_3$(Ce) scintillation detectors, Appl. Radiat. Isot. 63 (2) (2005) 223–228.
[13] B. Milbrath, R. Runkle, T. Hossbach, W. Kaye, E. Lepel, B. McDonald, L. Smith, Characterization of alpha contamination in lanthanum trichloride scintillators using coincidence measurements, Nucl. Instrum. Methods Phys. Res. Sect. A: Accel. Spectrom. Detect. Assoc. Equip. 547 (23) (2005) 504–510.
[14] F. Quarati, I. Khodyuk, C. van Eijk, P. Quarati, P. Dorenbos, Study of ^{138}La radioactive decays using $LaBr_3$ scintillators, Nucl. Instrum. Methods Phys. Res. Sect. A: Accel. Spectrom. Detect. Assoc. Equip. 683 (2012) 46–52.
[15] A. Camp, A. Vargas, J.M. Fernndez-Varea, Determination of $LaBr_3$(Ce) internal background using a {HPGe} detector and monte carlo simulations, Applied Radiation and Isotopes, Proceedings of the 20th International Conference on Radionuclide Metrology and its Applications 8–11 June 2015, Vienna, Austria, vol. 109, 2016, pp. 512–517.
[16] H. Negm, M. Omer, H. Zen, I. Daito, T. Kii, K. Masuda, T. Hori, H. Ohgaki, R. Hajima, T. Hayakawa, T. Shizuma, N. Kikuzawa, H. Toyokawa, Monte carlo simulation of response function for $LaBr_3$(Ce) detector and its internal-activity, in: Advancements in Nuclear Instrumentation Measurement Methods and their Applications (ANIMMA), 2013 Proceedings of the 3rd International Conference on, June 2013, pp. 1–5.
[17] W. Wolszczak, P. Dorenbos, Non-proportional response of scintillators to alpha particle excitation, IEEE Trans. Nucl. Sci., 2017, (in press).
[18] H. Bateman, The solution of a system of differential equations occurring in the theory of radioactive transformations, in: Proceedings Cambridge Philos. Soc, vol. 15, 1910, pp. 423–427.
[19] K. Skrable, C. French, G. Chabot, A. Major, A general equation for the kinetics of linear first order phenomena and suggested applications, Health Phys. 27 (1) (1974) 155–157.
[20] R. Brun, F. Rademakers, ROOT an object oriented data analysis framework, Nucl. Instrum. Methods Phys. Res. Sect. A: Accel. Spectrom. Detect. Assoc. Equip. 389 (12) (1997) 81–86 (New Computing Techniques in Physics Research V.).
[21] R. Ogawara, M. Ishikawa, Feasibility study on signal separation for spontaneous alpha decay in $LaBr_3$:Ce scintillator by signal peak-to-charge discrimination, Rev. Sci. Instrum. 86 (8) (2015).
[22] M.S. Alekhin, D.A. Biner, K.W. Krmer, P. Dorenbos, Improvement of $LaBr_3$:5%Ce scintillation properties by Li^+, Na^+, Mg^{2+}, Ca^{2+}, Sr^{2+}, and Ba^{2+} co-doping, J. Appl. Phys. 113 (22) (2013) (pp. -).